Level set X-FEM non matching meshes: application to dynamic crack propagation in elastic-plastic media

B. Prabel[1,2], A. Combescure [1], A. Gravouil [1] and S. Marie [2]

2006

1: LaMCoS, Laboratoire de Mecanique des Contacts et des Solides, UMR 5514, INSA Lyon, Bat. Jean d'Alembert, 18,20 rue des Sciences 69621 Villeurbanne France 2: DM2S/SEMT/LISN, CEA Saclay, 91191 Gif-sur-Yvette, France

Abstract

This paper develops two aspects improving crack propagation modeling with the X-FEM method. On the one hand, it explains how one can use at the same time a regular structured mesh for a precise and efficient level set update and an unstructured irregular one for the mechanical model. On the other hand, a new numerical scheme based on the X-FEM method is proposed for dynamic elastic-plastic situations. The simulation results are compared with two experiments on PMMA for which crack speed and crack path are provided.

Key words: extended finite element method, plasticity, level set, dynamic crack propagation, experiments

1 INTRODUCTION

The modelization of arbitrary crack propagation has seen major advances these last years, mainly because of the appearance of extended finite elements concepts.

Based on the concept of partition of unity introduced by Babuska and Melenk in [1], the eXtended Finite Element Method developed by Black *et al.* [2] incorporates in the interpolation of the displacement field the asymptotic behavior of the solution of a crack in an elastic media, so that fracture parameters are very well calculated. Moes *et al.* [3] enhanced this method adding a discontinuous part in the displacement field. This suppose to define implicitly the crack location. The level

sets method of Osher *et al.* [4] provides an efficient way of doing it, even in three dimensions (as demonstrated by Moes *et al.* [5] and Gravouil *et al.* [6]). Recent workers (as Belytschko *et al.* [7], De Borst [8], Réthoré *et al.* [9] or Menouillard *et al.* [10]) have still improved the method which has been extended to transient analysis of elastic crack propagation. It has mainly been shown that the method can be applied and ensures under certain conditions exact energy conservation even during crack propagation.

The method has nevertheless one main drawback which is linked to the propagation of level sets strategy, based on a finie difference concept whose precision is destroyed when the simulations are not done on a equally spaced or slowly varying spatial mesh.

Plasticity of material is an important dissipation mechanism and hence may severly modify the dynamic crack propagation (directions and speed). This is for example the case in [11], where an elastic plastic consitutive model is associated with the X-FEM kinematics to simulate shear band propagation. The first aim of this paper is to propose a numerical scheme which extend accurately the X-FEM elastic dynamic crack propagation simulations to elastic-plastic cases.

Level sets method loses efficiency when applied on triangulated domain. The proposed idea is to update the level set functions on a regular grid which is different from the structural mesh. By this method a very simple and efficient finite difference scheme can be directly used for level set propagation simulation.

The paper is organized as follows : in Section 2, the mechanical model of the X-FEM is presented. Section 3 details the changes due to the incorporation of a elastic-plastic law. Section 4 is dedicated to the level sets update and projection. Finally, numerical examples of dynamic crack propagation in elastic-plastic media are presented in Section 5, and compared to experimental results.

2 MECHANICAL MODEL

2.1 Equilibrium equations

We consider a material body Ω with a crack Γ (figure 1). The motion of the body is described by the displacement $\underline{u}(\underline{x},t)$ (where $\underline{x}$ is the position of material points). Displacement and velocity at time 0 are known as initial condition of the problem. We assume small perturbations, hence the strain tensor is :

$$\underline{\underline{\varepsilon}} = \frac{1}{2}\left(\underline{\underline{\nabla}}\left(\underline{u}\right) + \underline{\underline{\nabla}}^T\left(\underline{u}\right)\right) \tag{1}$$

where $\underline{u}$ is the displacement field and $\underline{\underline{\nabla}}$ is the gradient operator.

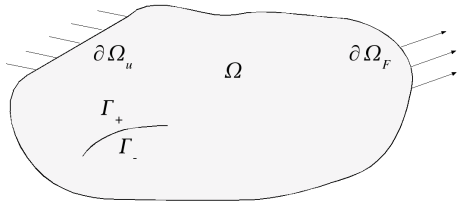

Figure 1: Body notation

The body is submitted to prescribed displacements $\underline{u_d}$ on the boundary $\partial\Omega_u$, to body forces $\underline{f_d}$ on Ω, and/or to external loads $\underline{F_d}$ on the boundary $\partial\Omega_F$. The crack faces Γ_+ and Γ_- are supposed to be traction free. $\underline{\underline{\sigma}}$ is the Cauchy stress tensor, and $\dot{} = \frac{\partial}{\partial t}$ denotes the time derivation.

The strong form of the problem is :

Find the stress and displacements $(\underline{\underline{\sigma}}, \underline{u})$ such that :

$$\underline{u} = \underline{u_d} \qquad \text{on } \partial\Omega_u \tag{2}$$

$$\text{div}(\underline{\underline{\sigma}}) + \underline{f_d} = \rho\underline{\ddot{u}} \qquad \text{in } \Omega \tag{3}$$

$$\underline{\underline{\sigma}} \cdot \underline{n} = \underline{F_d} \qquad \text{on } \partial\Omega_F \tag{4}$$

$$\underline{\underline{\sigma}} \cdot \underline{n} = \underline{0} \qquad \text{on } \Gamma_+ \cup \Gamma_- \tag{5}$$

The three last equations can be written in the weak form :

$$\forall \underline{v} \text{ in } V^0, \qquad \int_\Omega \rho\underline{\ddot{u}} \cdot \underline{v}\, d\Omega + \int_\Omega \underline{\underline{\sigma}} : \underline{\underline{\varepsilon}}(\underline{v})\, d\Omega = \int_\Omega \underline{f_d} \cdot \underline{v}\, d\Omega + \int_{\partial\Omega_F} \underline{F_d} \cdot \underline{v}\, d\Gamma \tag{6}$$

where $V^0 = \{v, \quad \underline{v} = 0 \quad \text{on } \partial\Omega_u\}$.

The constitutive equations have to be added to solve the problem.

2.2 Plasticity Equations

The material is assumed to be elastic-plastic. It can be described by the usual strain partition into elastic and inelastic parts :

$$\underline{\underline{\varepsilon}} = \underline{\underline{\varepsilon}}^e + \underline{\underline{\varepsilon}}^p \tag{7}$$

$$\text{where :} \qquad \underline{\underline{\varepsilon}}^e = D^{-1}\underline{\underline{\sigma}} \qquad \text{and} \qquad \dot{\underline{\underline{\varepsilon}}}^p = \begin{cases} 0 & \text{if } f(\underline{\underline{\sigma}}, R, \underline{\underline{X}}) < 0 \\ \underline{\underline{g}}(\underline{\underline{\sigma}}) & \text{if } f(\underline{\underline{\sigma}}, R, \underline{\underline{X}}) = 0 \end{cases} \tag{8}$$

In equations 7 and 8, $\underline{\underline{\varepsilon}}$ is the total strain, $\underline{\underline{\varepsilon^e}}$ the elastic part, $\underline{\underline{\varepsilon^p}}$ the inelastic one, $\underline{\underline{\dot{\varepsilon}^p}}$ the plastic strain rate, D is the Hooke matrix, $\underline{\underline{\sigma}}$ the stress, g the flow potential, f the plasticity criterion, whereas R and $\underline{\underline{X}}$ are two hardening variables. In this paper, standard Von Mises with isotropic hardening is used with an associated flow rule ($f = g$).

2.3 Time Discretization

The numerical time integration is based on the implicit Newmark mean acceleration scheme with parameters ($\gamma = \frac{1}{2}, \beta = \frac{1}{4}$). This scheme is unconditionally stable ([12]).

2.4 Space Discretization

2.4.1 Formulation.

The space discretization is based on the eXtended Finite Element Method ([5], [13]). New 4-noded elements have been developed in the software Cast3m © (developped by the French Commissariat à l'Energie Atomique [14]).

The displacement field is the sum of a standard continuous part (with the usual shape functions $N_i(\underline{x})$) and of an enriched part (containing discontinuous as well as singular functions).

$$\underline{u}(\underline{x}) \simeq \sum_{i \in I_0} N_i(\underline{x}) \cdot \underline{u}_i + \sum_{i \in I_1} N_i(\underline{x}) H(\underline{x}) \cdot \underline{a}_i + \sum_{i \in I_2} N_i(\underline{x}) \Big(\sum_{k=1,..4} F_k(\underline{x}) \cdot \underline{b}_{i,k} \Big) \quad (9)$$

I_0, I_1, I_2 are respectively the total set of nodes, the set of nodes whose support is intersected by the crack and that doesn't belong to I_2 , and the set of nodes of the element(s) that contains (or have contained previously) the crack tip(s). On figure 2 the symbol $\boxdot$ (resp.$\triangle$) represents nodes belonging to the set I_1 (resp. I_2).

The asymptotic fields of a crack propagating dynamically (with non-negligible inertial effect) in an elastic-plastic media are different from the elastic quasi-static ones. For example, in the static case of a monotonically increasing loading applied to a crack in a hardening material, Hutchinson, Rice, and Rosengren in [15] and [16] showed that stress fields were proportional to $r^{-\frac{1}{n+1}}$ (where n is the hardening exponent of the Ramberg-Osgood stress strain law, which equals 1 in the elastic case). Furthermore, the dynamic fields of a crack moving in an elastic media are velocity dependent [17].

In such a situation, there is no elementary analytical solution of the moving crack problem. Hence it was chosen to use the elastic static Weestergaard's basic

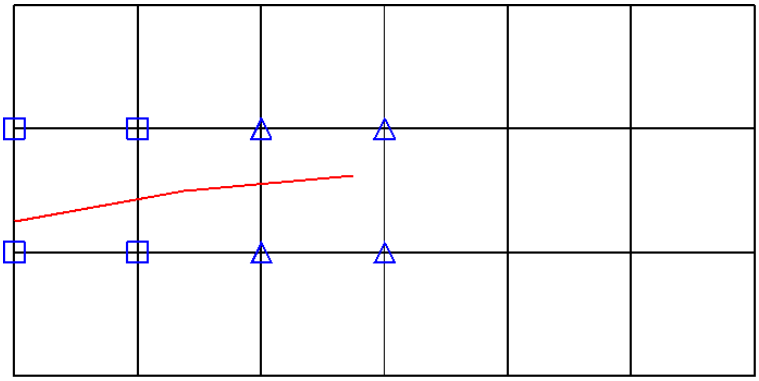

Figure 2: Enrichment strategy

functions (which can be found in [2]) to approximate the dynamic displacement and speed singularities at dynamic moving crack tip. Besides, the use of the Newmark scheme limits to the same space of functions the displacement, velocity and acceleration approximations.

2.4.2 Numerical integration.

The numerical integration of cut elements is generally performed by partitioning them into standard subtriangles. Hence every time the crack propagates, one uses a new set of subtriangles as well ad a new Gauss points set. This technique is valid for elastic crack propagation.

In case of an elastic-plastic media, the values of fields (stresses, inelastic strains, or internal variables) are computed at Gauss points. When the crack is not moving the sub element technique is the best strategy to compute the stress and strain state. When the crack moves either in static or in transient case the set of subtriangles has to be changed and a complex projection has to be performed each time the crack moves. This technique leads to a poor quality of the projected quantities and to complex field (stress and internal variable sets) transport when one changes the mesh. With this technique it is impossible to prove energy conservation when the crack propagates.

To avoid this, we choose to integrate enriched elements (it means cut elements, tip-elements, and their neighbors) with a larger number of Gauss points (typically 64) whose position is fixed in the element.

This integration strategy is developped in [18], where it is shown that it is sufficient to get an accurate tangent stiffness matrix. No locking of the degree of freedom corresponding to the singular enrichment has been observed, but non

transmissible ”hourglass” modes have been detected.

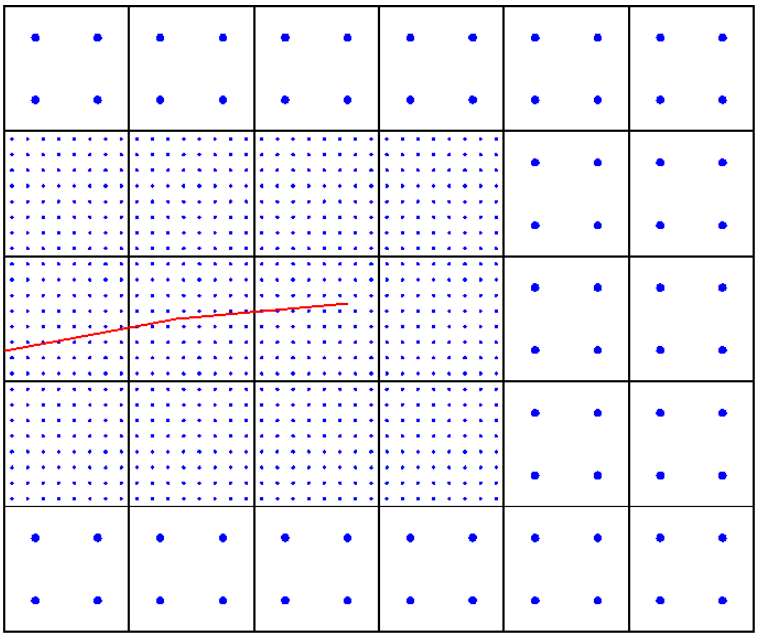

Figure 3: Numerical integration

The projection of the fields from a 4-Gauss points element to a 64-Gauss point element anticipates the arrival of the crack tip in the element as it can be observed on figure 3. These elements are integrated with a richer Gauss points set before they are reached by crack tip plastic field. This technique introduces a small error in the element integration but is prefered because it does not imply any field projection close to crack tip where the fields are very rapidly changing. In case of plasticity confined to the crack tip the change of Gauss point sets is done in elements which are still elastic. Since the new degree of freedom are set to zero, no supplementary strain energy is introduced.

To demonstrate that the quadrature technique meet quality requirements, stress intensity factors K_I and K_{II} of an inclined crack in an infinite body in traction are evaluated through the interaction integral. Half crack length a is taken as $1/100$ of the total plate dimension, and the mesh size in the crack tip vicinity is equal to $a/10$. With this method the results on stress intensity factors appear to be of good quality for any position of the crack within the element. Figure 4 shows the quality of the solution for various inclinaison angle (from $0°$ to $90°$). Values are normalized by $\sigma^\infty\sqrt{\pi a}$, where σ^∞ is the applied stress.

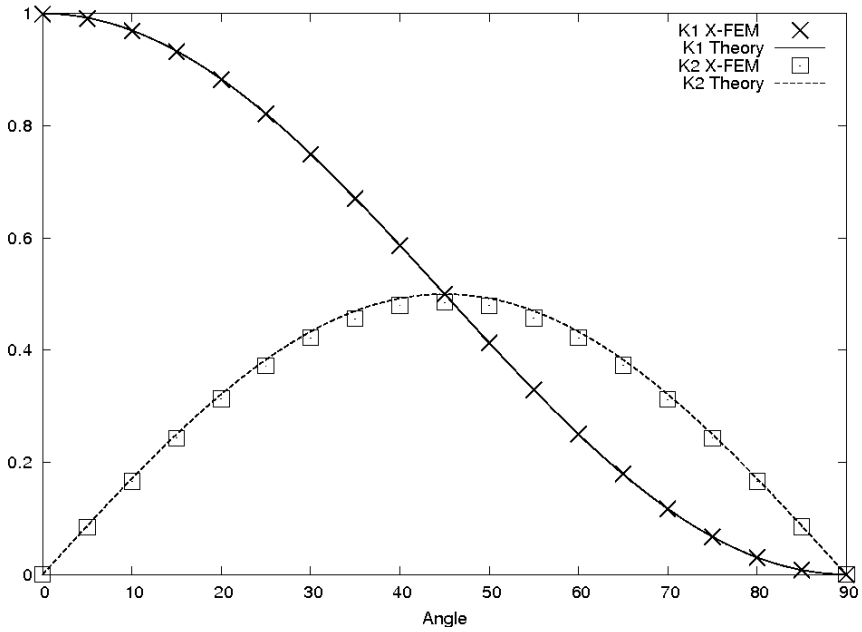

Figure 4: Stress intensity factors with respect to the angle of the inclined crack

2.5 Resolution

Injecting the time and space discretization into equation (6) and taking into account the material behavior (equations (7) and (8)), we get a non linear system that is solved with a Newton-Raphson iterative scheme.

The boundary conditions are fulfilled with the Lagrange multipliers' technique.

3 CRACK GROWTH IN ELASTIC-PLASTIC MEDIA

3.1 Dynamic crack propagation in elastic media

X-FEM method enables to model dynamic crack propagation in elastic media in an efficient way. After the determination of the crack direction and velocity, level sets functions are updated to define implicitly the new crack position. To the new configuration of the crack correspond new degrees of freedom which are simply added to the previous one. Their initialization to zero guarantees that no numerical energy is introduced as proved in [9].

3.2 Fracture mechanics parameters calculation

The J-integral introduced by Rice is calculated in dynamic via the G-Theta method (see [19] and [20]).

$$J = \int_\Omega \left(-(w^{def} + w^{cin})\delta_{jk} + \sigma_{ij} u_{i,k} \right) q_{k,j} \, d\Omega + \int_\Omega (\rho \ddot{u}_i u_{i,k} - \rho \dot{u}_i \dot{u}_{i,k}) q_k \, d\Omega \tag{10}$$

where $w^{def} = \int_0^{\varepsilon_{ij}} \sigma_{ij} : d\varepsilon_{ij}$, $w^{cin} = \frac{1}{2}\rho \dot{u}_i \dot{u}_i$. and $\underline{q}$ is an arbitrary smooth function whose direction is the same of the crack and whose norm is 1 in a domain surrounding the crack tip and goes to 0 out of a larger domain. A representation can be found on figure 5. This formulation is in accordance with the J-integral

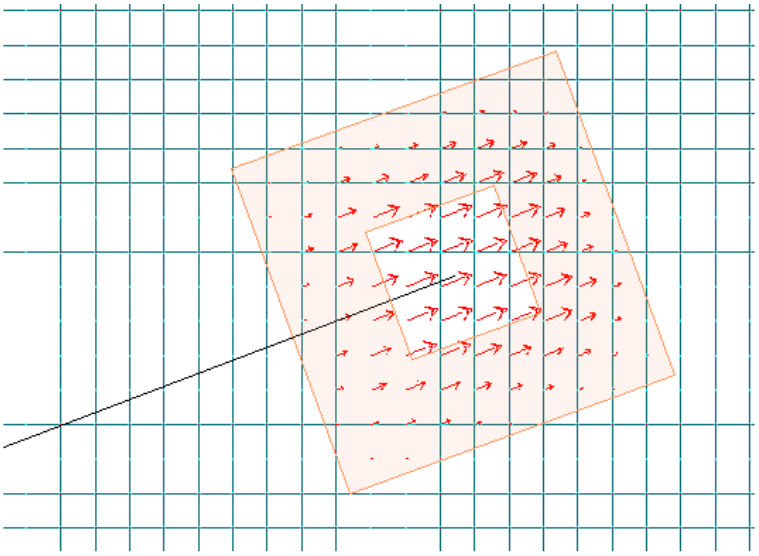

Figure 5: $\underline{q}$-domain for an inclined crack (20°). Shaded area represent the region where $\underline{\underline{\nabla} q}$ is not nul.

defined by Bui in [21] and the flux integral of Freund [17]. In case of turning or branching crack, the interaction integral concept is used to determine the stress intensity factors. Its expression is derived from the J-integral (10) and can be found in [22] or in [9]. The asymptotic fields used here are these of a stationnary crack. These concepts are valid in case of elastic or of plastic zones very confined to the crack tip. They shall also be used in case of extensive yielding: this hypothesis can be considered as very crude but it has the advantage of being a ”global” parameter less sensitive to ”local” criterium (for instance computed using the stress values at the closest Gauss points to the crack tip whose numerical quality is rather poor)

which are very often used to decide crack propagation speed as well as direction.

3.3 Crack growth model

To determine the crack speed, one can invert the empirical dynamic toughness relation given by Kanninen *et al.* [23] and get the following equation :

$$\dot{a} = \begin{cases} 0 & \text{if } K^{dyn} \leq K_c \\ V_l\Big(1 - \frac{K_A}{K^{dyn}}\Big)^{\frac{1}{m}} & \text{if } K^{dyn} > K_c \end{cases} \tag{11}$$

If the simulation provides an equivalent dynamic stress intensity factor K^{dyn} greater than the toughness K_c, then the crack speed can be determined by the previous equation. The lack of experimental data leads to the following hypothesis :

1. Fracture initiation and arrest toughness are the same ($K_c = K_A$).
2. The limiting crack speed is equal to the Rayleigh wave speed ($V_l = c_r$).
3. The coefficient m is equal to 1.

K^{dyn} may be viewed as the equivalent dynamic stress intensity factor, which is defined as the asymptotic value of the hoop stress and can be expressed as a combination of K_I^{dyn} and K_{II}^{dyn}. These last two terms can be determined using the interaction integral method in the elastic case.

An alternative method consists to assume the mode II negligible and use the J integral to calculate G. In dynamic case the relationship between the energy release rate and the stress intensity factors depends upon the crack speed via the universal functions : $G = \frac{1}{E^\star}\left[A_I(\dot{a})K_I^2 + A_{II}(\dot{a})K_{II}^2\right]$. This leads to a non linear equation to solve to get the crack speed.

The direction of propagation is chosen to be driven by the maximum hoop stress which can be expressed in terms of stress intensity factors by the following equation:

$$\theta = 2\, atan\left[\frac{1}{4}\left(\frac{K_I^{dyn}}{K_{II}^{dyn}} - \; sign\left(K_{II}^{dyn}\right)\left[\left(\frac{K_I^{dyn}}{K_{II}^{dyn}}\right)^2 + 8\right]^{\frac{1}{2}}\right)\right] \tag{12}$$

It can be quoted here that this simple crack growth model, based on the hypothesis of plasticity confined to the crack tip, remains valid in most cases, even if some improvements may be further investigated.

4 LEVEL SET UPDATE

4.1 Auxiliary grid

Practical industrial structures cannot in general be described by a structured regular mesh, even if one can use X-FEM concepts to define the contour (as done in [24]). When one needs to update the crack position in the mechanical model, one needs to update the level set functions (see [6] for more details). But, level set update on an unstructured irregular mesh requires the use of special algorithms for triangulated domain (e.g. Petrov Galerkin's scheme [25]) which is a bit sophisticated. In order to get a general frame for computation of complex geometries with simple level set grids it has been chosen to use two different meshes:

1. A standard finite element unstructured mesh for the mechanical computation
2. An auxiliary regular structured one for the level set representation.

This last mesh can be concentrated only in the regions where the crack is going to grow and is completly independent from the finite element mesh. Hence, the introduction of this auxiliary structured grid permits us to use very simple schemes (like Godunov's one) based on finite difference approximation.

First, the mechanical model gives us speed and direction of crack propagation. These scalars are the same for the regular grid. So update, reinitialization, and orthogonalization can be done in an efficient way on the regular grid. Crack update is made by solving at each point (i, j) of the finite difference grid :

$$\frac{\partial \psi}{\partial t} = V_\psi \cdot ||\nabla \psi|| \tag{13}$$

with :

$$\frac{\partial \psi_{(i,j)}}{\partial t} = \frac{\psi^{t+\Delta t}_{(i,j)} - \psi^{t}_{(i,j)}}{\Delta t} \tag{14}$$

$$(V_\psi \cdot ||\nabla \psi||)_{(i,j)} = max\left\{V_{(i,j)}, 0\right\} \cdot \nabla^+ + min\left\{V_{(i,j)}, 0\right\} \cdot \nabla^- \tag{15}$$

∇^+ and ∇^- are two functions of $\psi^t_{(m,n)}$ where $m = \{i-1, i, i+1\}$ and $n = \{j-1, j, j+1\}$. Their expression can be found in [4], [26] and [27].

t is the instant considered for the update and Δt the time step.

4.2 Projection onto the mechanical mesh

Once the new level set functions are determined on the auxiliary grid, a projection step gives their value on the mechanical mesh. The approximation functions used for this projection are the standard finite element approximation. The value of the

level set ψ at a node p of the mechanical mesh whose coordinate $\underline{x}^p$ are within the 4-nodes element e of the level set grid is given by the following interpolation equation:

$$\psi(\underline{x}^p) \simeq \sum_{i=1,4} N_i(\underline{x}^p) \cdot \psi_i^e \tag{16}$$

Concerning the mesh size, the following remarks can be done :

1. To take curvature effect into account in the level set update, the grid size should be sufficiently small (typically one tenth of the radius of curvature to get a relative error around few percents).

2. In order to keep accurate crack geometry information during the projection step, the mechanical mesh size should be close to the auxiliary grid's one. It leads to propose the practical rule :

$$\Delta x_{auxiliary\ grid} \ \sim \ min(\Delta x_{mechanical\ mesh}) \tag{17}$$

The calculation cost is very reasonable because the level set update requires no matrix inversion. The algorithm is fully explicit. The only restriction is the time step.

The use of such a grid permits to define the level set functions only where the crack can possibly grow. This point is similar to the narrow band method developed by Sethian [26], and adapted by Ventura *et al.* in [28] and [29].

5 NUMERICAL EXAMPLE

5.1 Original experiments

The numerical examples comes from the experiments of Gregoire *et al.* [30].

A PMMA specimen is put between two Hopkinson bars as shown on figure 6. A hole with a notch permits to the compression wave to initiate a crack in mixed mode loading depending on the geometric configuration. Strain is measured for the input and output bar. It gives information about the loading that can be interpreted in speed or strength term. Photographs are made and interpreted to determine the crack position at different times.

Two computations have been done with different meshes of 8000 and 12000 nodes, which give sensibly the same results. We present here the results given by the finer mesh. For sake of clarity, example of mechanical and level set meshes containing about 8000 nodes is displayed on figure 7.

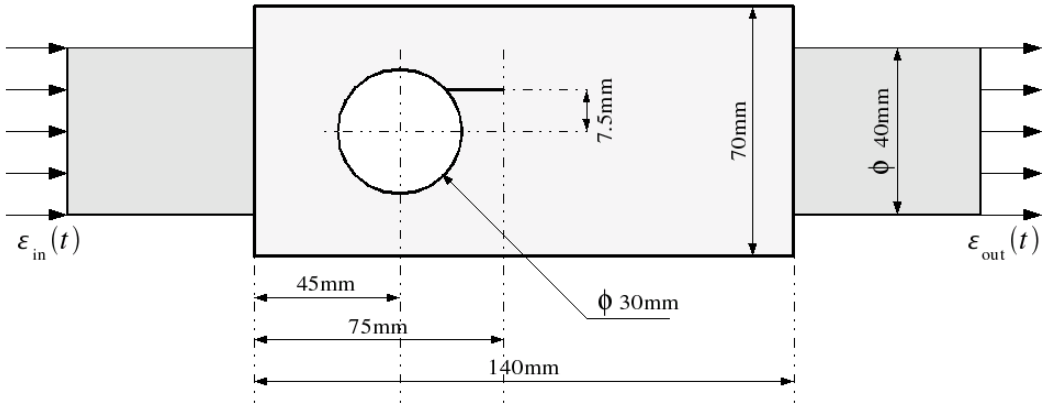

Figure 6: Experimental configuration, first specimen type

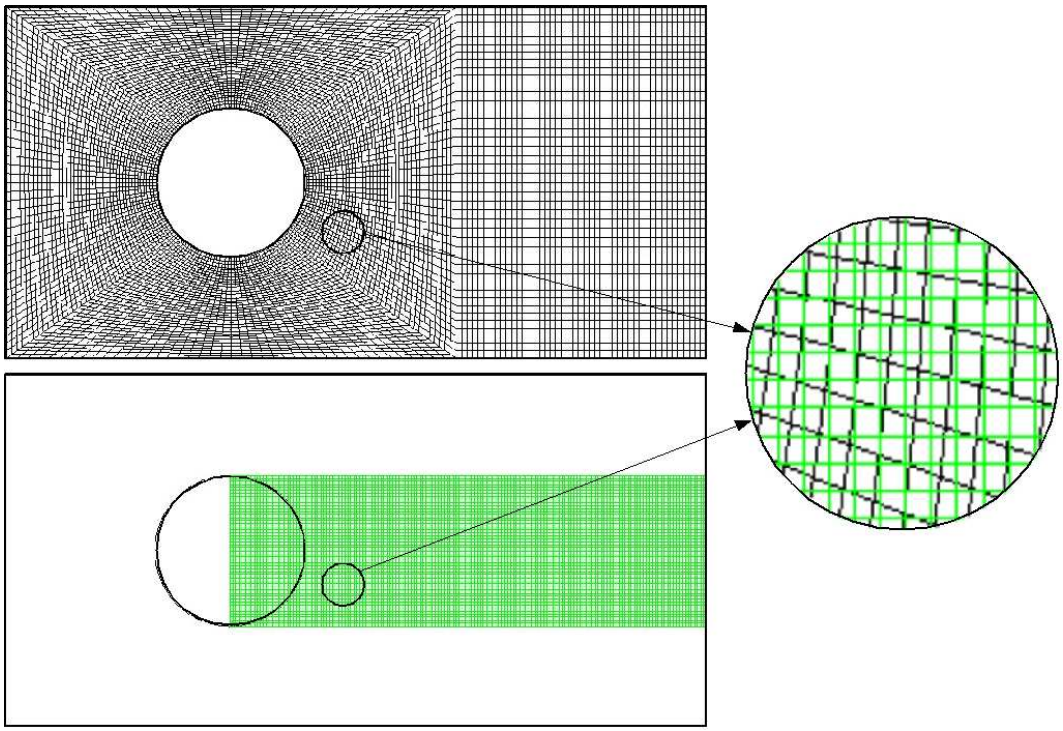

Figure 7: Unstructured mechanical mesh (top), regular level set grid (bottom)

The computations are done using the plane strain option.
We shall study two different specimen which differ only by the crack geometry.

The first one is represented on figure 6 and is discussed in the following paragraphs, whereas the second one contains two cracks which may interact, is displayed on figure 13 and is presented in the last paragraph of this section.

5.2 Boundary conditions

We impose the velocity $\dot{u}_x(t)$ of the left side of the specimen to be equal to the experimental value recorded, and add a force proportional to the velocity of the right side in order to simulate the action of the second Hopkinson bar. This last condition is given as in [30] by the following equation : $F_x^{ext} = -z\dot{u}_x$ where the impedance z can be evaluated to : $z = \sqrt{\rho E}$. As figure 8 shows it, the impedance boundary

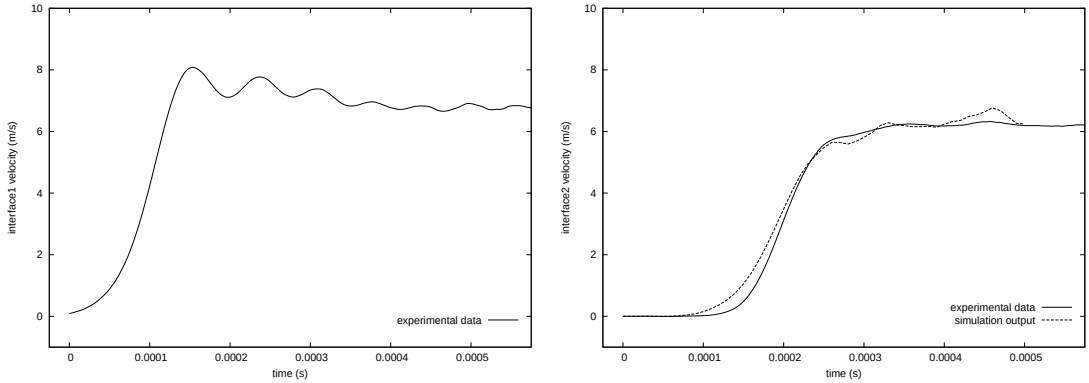

Figure 8: Velocity of the left side, and velocity of the right side

condition permits to calculate right side velocity very close to the experimental data.

5.3 Material properties

We suppose the material to have strain rate independant properties with the values reported in the following table.

E	ν	ρ	K_{Ic}	σ_Y
$3.0\,GPa$	0.42	$1180\,kg.m^{-3}$	$1.2\,MPa\sqrt{m}$	$80MPa$

In this table, E is the Young's modulus, ν the Poisson's ratio, ρ the volumetric mass, K_{Ic} the fracture toughness, and σ_Y the yield stress. The material is supposed to be perfectly plastic which is a reasonable hypothesis for the PMMA.

5.4 Elastic-Plastic crack growth prediction

This experiment has two very interesting outcomes: First the crack path which is rather complex, and second the fact that the crack stops during a significant time and the starts again to propagate. We first compare the evolutions of the experimental crack tip length to the computed ones obtained for different yield equivalent stresses. The crack length as a function of time is displayed of figure 9 and compared to the computed ones. One can see that the crack first propagates at constant speed then stops between 0.25ms to 0.32ms and then propagates again at roughly the same speed. With elastic or reasonable yield equivalent stress of 80 MPa, the introduction of an elastic-plastic behavior doesn't really change the global computed response of the specimen (figure 9). The crack path are very similar to the experimental one (figure 11). It can hence be concludes that crack propagates with small scale yielding.

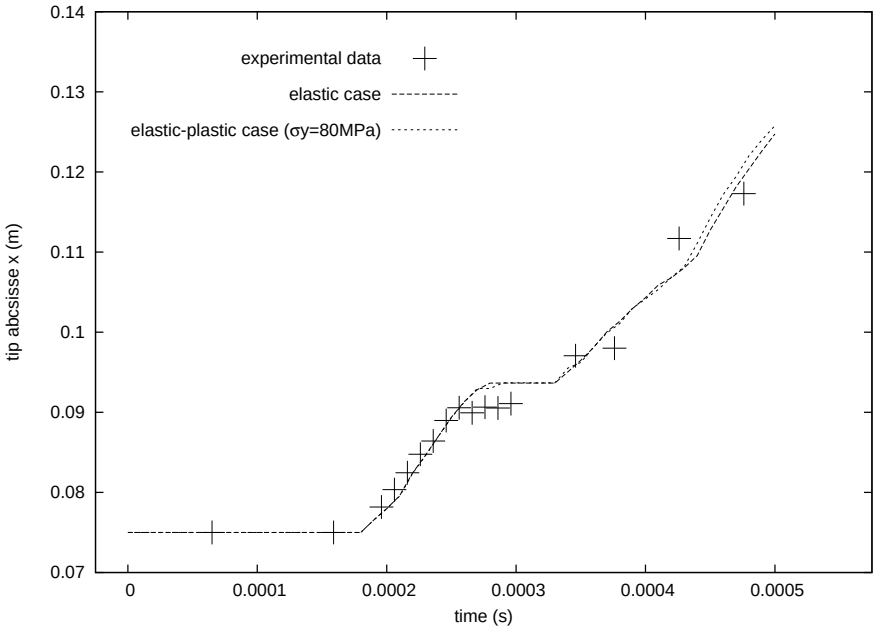

Figure 9: Crack tip evolution with time

To understand the influence of the yield stress on the specimen's response, we have chosen to decrease this material parameter to 40, 20 and 10MPa. Results for 20 and 10MPa are displayed in this paper. It was observed that the crack does not stop any more when σ_Y is 20MPa and propagates at a lower speed when it is reduced to 10MPa (figures 10 and 11). It can also be noticed that the transmitted

wave drops in amplitude.

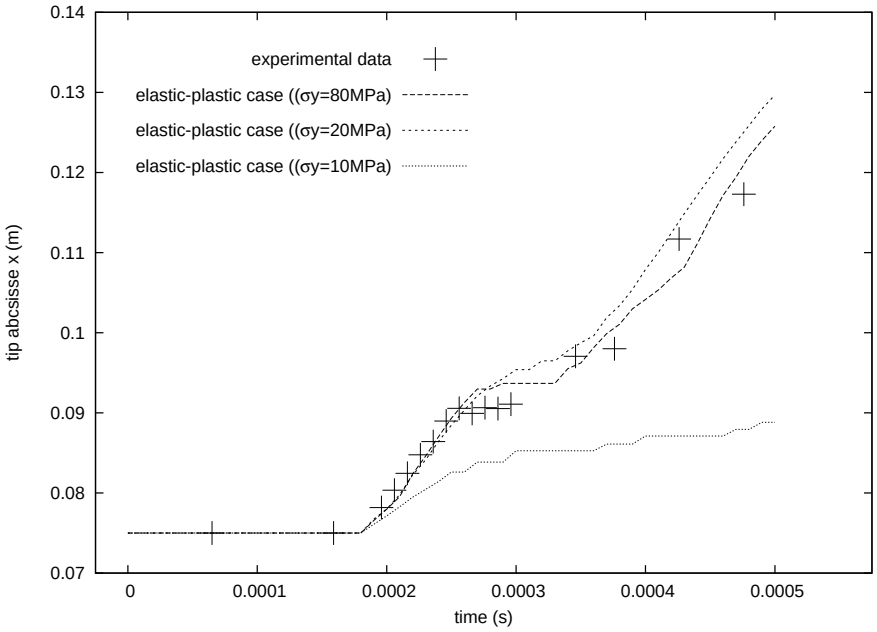

Figure 10: Crack tip evolution with time in elastic-perfectly plastic media

For a yield stress between 15 MPa and 10 MPa the plastification of the specimen becomes the main dissipation source and the crack hardly propagates.

Figure 12 displays the plastic zones. There are three zones. The first one is due to the boundary condition which develops shear band from the left side to the hole. The second one comes from the contraction of the specimen and appears around the hole. The third one is related to the usual plastic zone surrounding the crack tip.

We can conclude that in case of a yield equivalent stress of $\sigma_y \geqslant 40$MPa, the plastic zone is sufficiently small to consider this case as a small scale yielding situation. This is not the case with a lower yield stress.

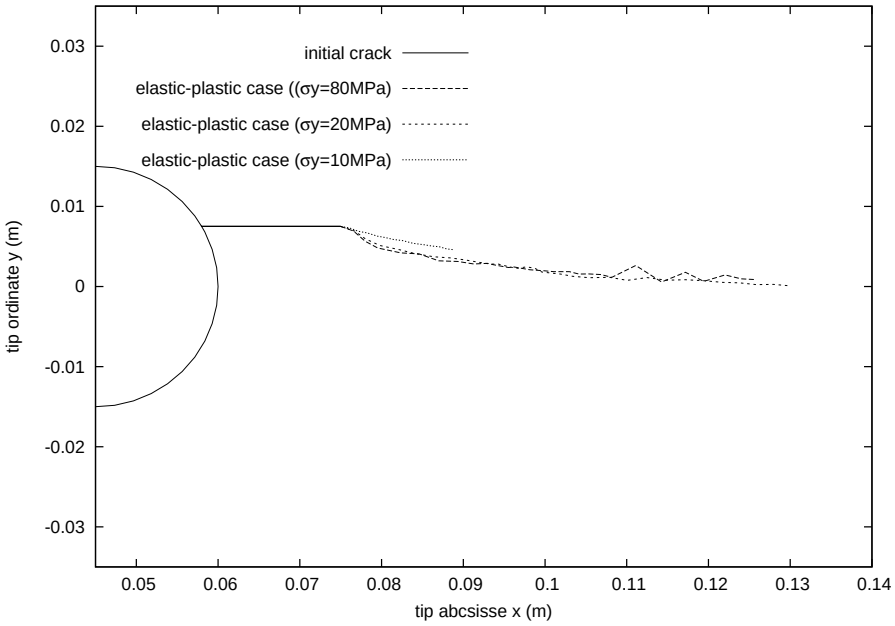

Figure 11: Crack path

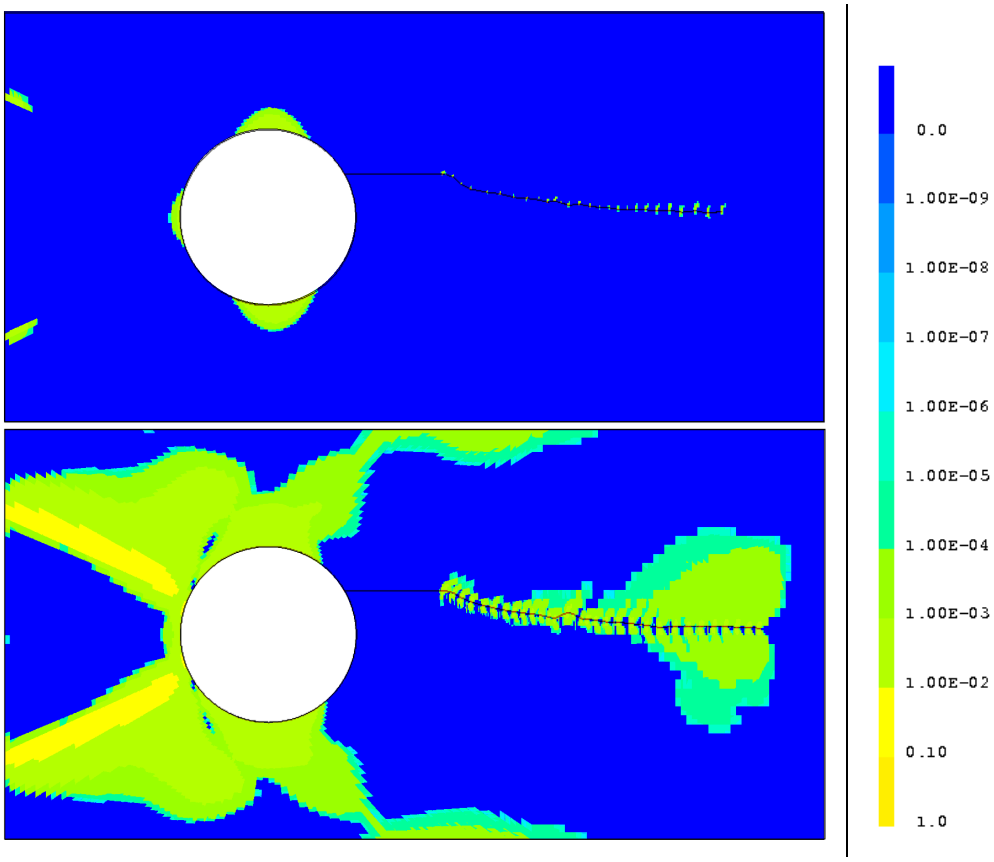

Figure 12: Equivalent inelastic deformation for $\sigma_y = 40$ MPa (top) and for $\sigma_y = 15$ MPa (bottom)

5.5 Second specimen type

The second PMMA specimen has two symmetrical notch which are radial to the hole. Their length and position is indicated on figure 13.

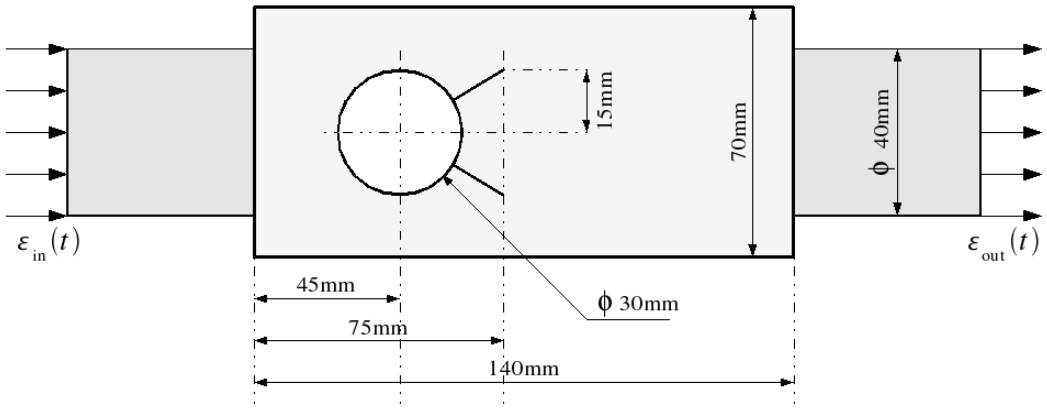

Figure 13: Experimental configuration, second specimen type

Results are similar to the previous specimen except that no arrest can be observed. As long as the yield equivalent stress is above 40 MPa, there's no obvious differences between the elastic and the elastic-plastic case.

Concerning the plastic zone, we observe that the equivalent inelastic strain is important at the initial crack tip (figure 16). It can be attributed to the large kink that occurs in the beginning of crack propagation (the change of direction is about 70°). The cracks do not collapse to a single one in accordance with what has been observed experimentally.

6 CONCLUSION

In this paper, it was demonstrated that the modelization of a propagating crack in an elastic-plastic media can be done using X-FEM linear functions approximation. Simulations show good agreement with experimental results, even if the material behavior isn't perfectly known. It opens the perspectives of complete dynamic elastic-plastic fracture simulation.

The use of an auxiliary structured grid to update the level set functions presents the advantages of high accuracy and easy programming.

Acknowledgments The support of French Commissariat à l'Energie Atomique is gratefully acknowledged.

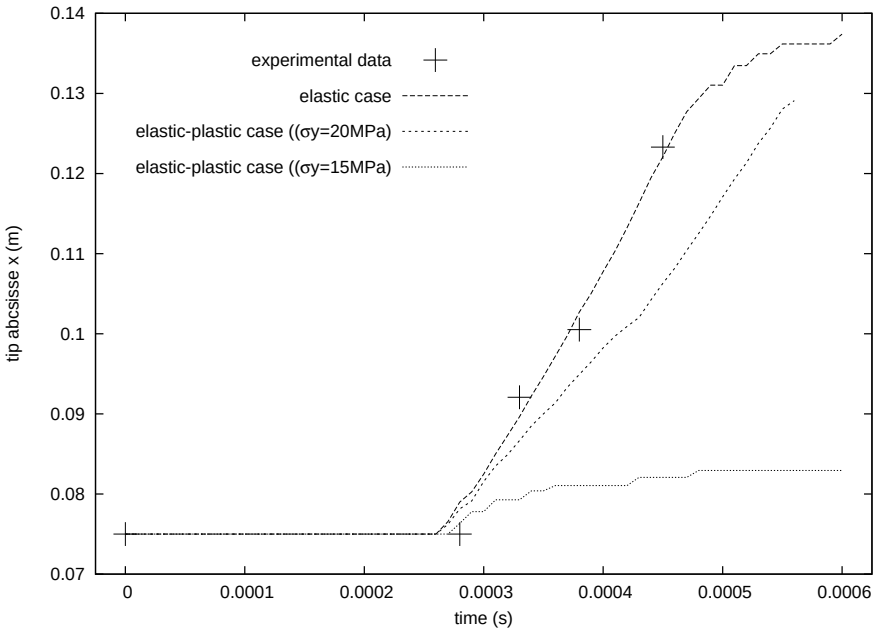

Figure 14: Crack tip evolution with time in elastic-perfectly plastic media

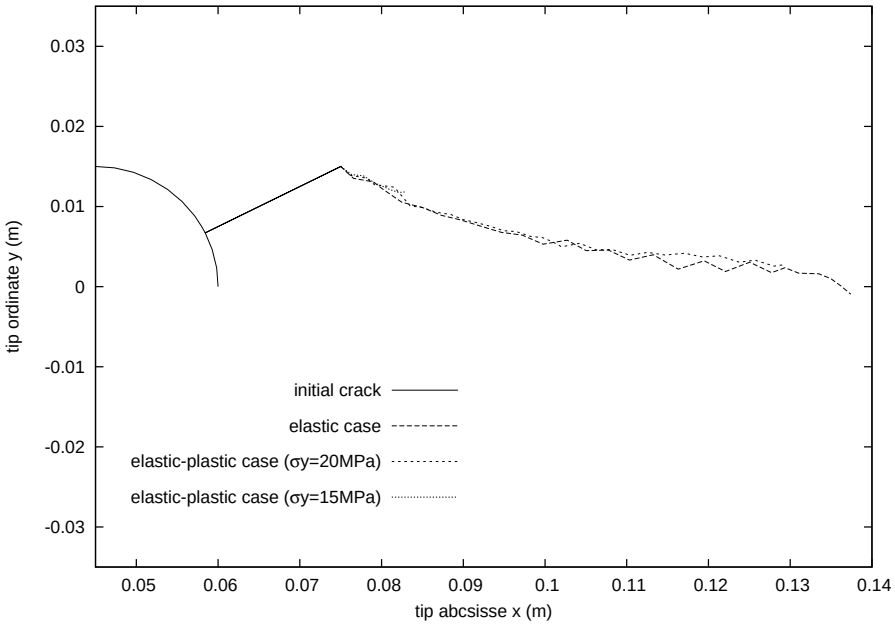

Figure 15: Crack path

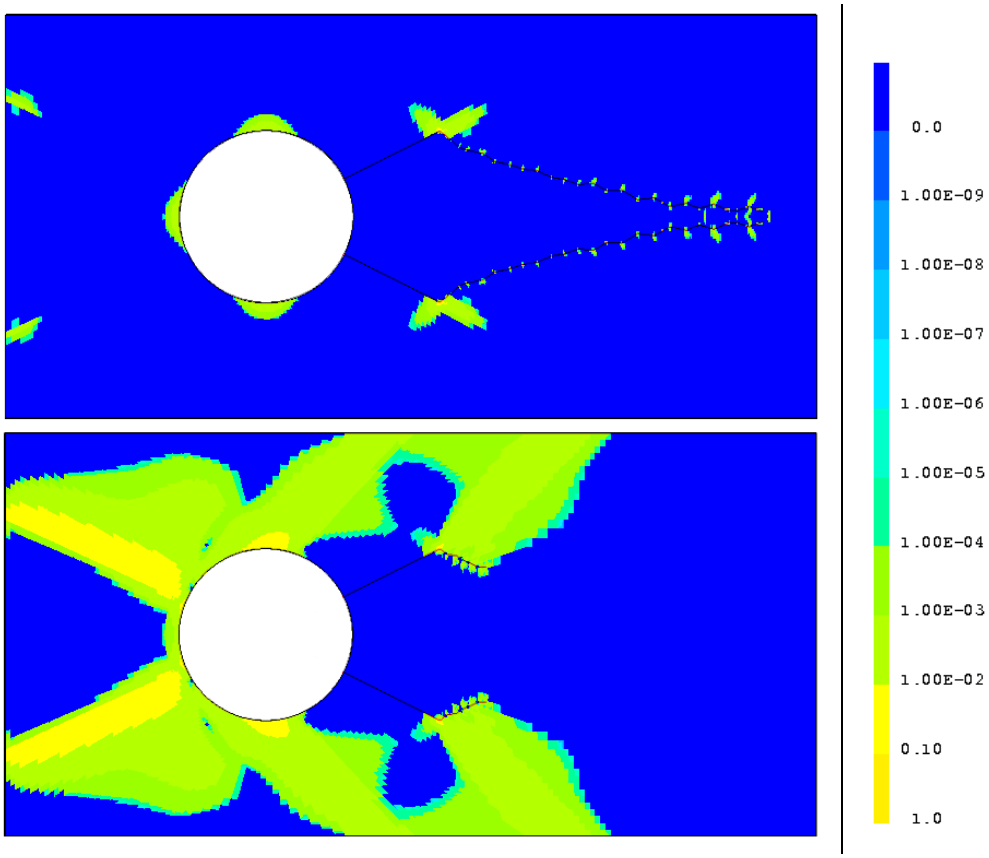

Figure 16: Equivalent inelastic deformation for $\sigma_y = 40$ MPa (top) and for $\sigma_y = 15$ MPa (bottom)

References

[1] I Babuska and J M Melenk. The partition of unity method. *International Journal of Numerical Methods in Engineering*, 40:727–758, 1997.

[2] T Black and T Belytschko. Elastic crack growth in finite element with minimal remeshing. *International Journal of Numerical Methods in Engineering*, 45:601–620, 1999.

[3] N Moes, J Dolbow, and T Belytschko. A finite element method without remeshing. *International Journal of Numerical Methods in Engineering*, 46:131–150, 1999.

[4] S Osher and J A Sethian. Fronts propagating with curvature-dependent speed: algorithms based on hamilton-jacobi formulations. *Journal of Computational Physics*, 79:12–49, 1988.

[5] N Moes, A Gravouil, and T Belytschko. Non planar 3d crack growth by the extended finite element and level sets : Part i : Mechanical model. *International Journal of Numerical Methods in Engineering*, 53:2549–2568, 2002.

[6] A Gravouil, N Moes, and T Belytschko. Non planar 3d crack growth by the extended finite element and level sets : Part ii : Level set update. *International Journal of Numerical Methods in Engineering*, 53:2569–2586, 2002.

[7] T Belytschko, H Chen, J Xu, G Zi, and R DeBorst. Dynamic crack propagation based on loss of hyperbolicity and a new discontinuous enrichment. *International Journal of Numerical Methods in Engineering*, 58:1873–1905, 2003.

[8] R DeBorst. Some recent issues in computational failure mechanics. *International Journal of Numerical Methods in Engineering*, 52:63–95, 2001.

[9] J Réthoré, A Gravouil, and A Combescure. An energy conserving scheme for dynamic crack growth with the extended finite element method. *International Journal of Numerical Methods in Engineering*, 63:631–659, 2005.

[10] T Menouillard, J Réthoré, and A Combescure. Explicit time stepping with xfem (submitted in 2005). *International Journal of Numerical Methods in Engineering*.

[11] E Samaniego and T Belytschko. Continuum discontinuum modelling of shear band. *International Journal of Numerical Methods in Engineering*, 62:1857–1872, 2005.

[12] N M Newmark. A method of computation for structural dynamics. *Proc. A.S.C.E.*, 85:67–94, 1959.

[13] M Jirasek. Numerical modeling of strong discontinuies. *Revue française de génie civil*, 6:1133–1146, 2002.

[14] Cast3m web page.

[15] J W Hutchinson. Singular behaviour at the end of a tensile crack in a hardening material. *Journal of Mechanics and Physics of Solids*, 16:13–31, 1968.

[16] J R Rice and G F Rosengren. Plane strain deformation near a crack tip in a power law hardening material. *Journal of Mechanics and Physics of Solids*, 16:1–12, 1968.

[17] L B Freund. *Dynamic fracture mechanics, Cambridge University Press*. 1989.

[18] T Elguedj, A Gravouil, and A Combescure. Appropriate extended functions for xfem simulation of plastic fracture mechanics. *Computer Methods in Applied Mechanics and Engineering*, 195:501–515, 2006.

[19] P Destuynder, M Djoua, and S Lescure. Some remarks on elastic fracture mechanics. *Journal de Mechanique Théorique et Appliquée*, 2:113–135, 1983.

[20] X Z Suo and A Combescure. Second variation of energy and an associated line independent integral in fracture mechanics. *European Journal of Mechanics, A/Solids*, 11:609–624, 1992.

[21] H D Bui. *Mecanique de la rupture fragile, Masson*. 1978.

[22] P Krysl and T Belytschko. The element free galerkin method for dynamic propagation of arbitrary 3-d cracks. *International Journal of Numerical Methods in Engineering*, 44:767–800, 1999.

[23] M F Kanninen and C H Popelar. *Advanced fracture mechanics, Oxford University Press*. 1985.

[24] N Sukumar, D L Chopp, N Moes, and T Belytschko. Modeling holes and inclusions by level sets in the xfem. *Computer Methods in Applied Mechanics and Engineering*, 190:6183–6200, 2001.

[25] T J Barth and J A Sethian. Numerical schemes for the hamilton-jacobi and level set equations on triangulated domains. *Journal of Computational Physics*, 145:1–40, 1998.

[26] J A Sethian. *Level set methods and fast marching methods, Cambridge University Press.* 1999.

[27] D Peng, and S Osher B Merriman, H Zhao, and M Kang. A pde-based fast local level set method. *Journal of Computational Physics*, 155:410–438, 1999.

[28] G Ventura, J X Xu, and T Belytschko. A vector level set method and a new discontinuity approximations for crack growth by efg. *International Journal of Numerical Methods in Engineering*, 54:923–944, 2002.

[29] G Ventura, E Budyn, and T Belytschko. Vector level sets for description of propagating cracks in finite element. *International Journal of Numerical Methods in Engineering*, 58:1571–1592, 2003.

[30] D Gregoire, H Maigre, and J Réthoré. Simulation with xfem of dynamic crack propagation under combined loading, comparison with experiments (submitted in 2006). *Journal of the Mechanics and Physics of Solids.*